GEOPHYSICAL RESEARCH LETTERS, VOL. 25, NO.12, PAGES 2053-2056, JUNE 15, 1998

The association of electrostatic ion cyclotron waves, ion and electron beams and field-aligned currents: FAST observations of an auroral zone crossing near midnight

C. Cattell[1], R. Bergmann[2], K. Sigsbee[1], C. Carlson[3], C. Chaston[3], R. Ergun[3], J. McFadden[3], F. S. Mozer[3], M. Temerin,[3] R. Strangeway[4], R. Elphic[5], L. Kistler[6], E. Moebius[6], L. Tang[6], D. Klumpar[7], R. Pfaff[8]

ABSTRACT. FAST particle and wave data for a single nightside auroral zone crossing are utilized to examine the free energy source for electrostatic ion cyclotron (EIC) waves. Comparisons of the unstable wave modes, obtained by an electrostatic linear dispersion relation solver, to the observed waves for two intervals with upflowing ion beams and two with upflowing electron beams are consistent with the conclusion that the observed waves near the cyclotron frequencies are EIC which are driven by the electron drift both in the upgoing ion beam regions and in the upgoing electron regions. A limitation is that the drifting bi-Maxwellian model used in the dispersion relation is not a good match to the observed upflowing electron distributions. The observed ion beams do not drive EIC waves; however, the relative drift of the various ion species comprising the ion beam can drive low frequency (<~50 Hz) waves unstable. The electron drift, during some intervals, also destabilizes electron acoustic waves.

1. Introduction

Electrostatic ion cyclotron (EIC) waves have been observed on auroral field lines by many satellites including S3-3 [*Kintner et al.*, 1978, 1979; *Temerin et al.*, 1979], ISEE-1 [*Cattell et al.*, 1991], Viking *[Andre et al.*, 1987] and Polar [*Mozer et al.*, 1997]. The waves are usually associated both with field-aligned currents and upflowing ion beams [*Kintner et al.*, 1979; *Cattell*, 1981; *Cattell et al.*, 1991]. Currents, ion beams, and velocity shear have all been proposed to provide the free energy for the instability [*Kindel and Kennel*, 1971; *Hauck et al.*, 1978; *Bergmann*, 1984; *Ganguli et al.*, 1988]. In addition, some studies suggest that the observed electrostatic waves near the various ion gyrofrequencies may be due to relative streaming between ion species [*Bergmann et al.*, 1988; *Kaufmann et al.*, 1986; *Dusenbury et al.*, 1988]. Although these waves have been extensively studied, the resolution of the data and lack of information on the background electron density and temperature have not allowed the definitive identification of the free energy source for the waves.

In this letter, we describe observations of waves near the cyclotron frequencies of H^+, O^+, and He^+ and the associated particle distribution functions and field-aligned currents during one nightside auroral zone crossing by the FAST satellite [*Carlson et al.*, 1998a]. The particle data are used to model input distributions for an electrostatic dispersion relation solver. The linear stability properties of the model plasma are then compared to observed wave characteristics to determine the wave modes and free energy source.

2. Observations

Figure 1 presents an overview of 3 minutes of data obtained as FAST moved poleward through the auroral zone and into the polar cap at an altitude of ~3800 to 4000 km near midnight magnetic local time on January 13, 1997 at 10:15. The electron pitch angle and energy spectra are plotted in panels a and b, and the ion spectra in panels c and d. Two regions of ion beams occurred (see peaks in the pitch angle spectrum at 180° in panel d). The beam composition was variable, including a large fraction of both O^+ and He^+. There were also many regions of intense upflowing electron beams (panel b; see *Carlson et al.*, 1998b). The signatures of three field-aligned current sheets can be seen in the eastward component of the magnetic field (panel e). The most equatorward (during the first ion beam) is upward, followed by a downward current sheet (with smaller scale embedded upward currents) during the interval of upward electrons, and, finally, a small scale upward current at the poleward edge of the auroral zone. The current densities were ~2-4 x 10^{-7} A/m^2, assuming that the observed change in the field was primarily due to the motion of the satellite rather than the motion of the current sheets. The power in the electric field component along the spacecraft velocity vector, approximately perpendicular to the geomagnetic field, (panel f) indicates that there were several bursts of waves (~10:17:40 and ~10:19:20) near the H^+ cyclotron frequency(f_{cH} ~ 205 Hz), the He^+ cyclotron frequency (f_{cHe} ~51Hz), the oxygen cyclotron frequency (f_{cO} ~ 13 Hz) and their harmonics. The rest of the emissions were less structured, showing either very broadband or low frequency waves. The

[1]School of Physics and Astronomy, University of Minnesota, Minneapolis, MN
[2]Department of Physics, Eastern Illinois University, Charleston, IL
[3]Space Sciences Laboratory, University of California, Berkeley, CA
[4]Institute of Geophysics and Planetary Physics, University of California, Los Angeles, CA
[5]Space and Atmospheric Sciences, Los Alamos National Lab Los Alamos, NM
[6]University of New Hampshire, Durham, NH
[7]Lockheed/Martin Research Laboratory, Palo Alto, CA
[8]NASA/GSFC, Laboratory for Extraterrestrial Physics, Greenbelt, MD

Paper number 98GL00834.
0094-8534/98/98GL-00834$05.00

waves and distributions will be examined in detail during four intervals: (1) 10:16:34, during the long duration ion beam and downgoing electron inverted V; (2) 10:17:37-10:17:41, during an intense upflowing electron beam with a clear beam; (3) 10:19:05, during a more typical upward electron event which also had counterstreaming; and (4) 10:19:17 -10:19:22, during the ion beam near the polar cap boundary.

To understand the waves, it is necessary to examine the time series data, as well as the spectra. Characteristic waveforms obtained during each of the selected intervals are plotted in Figure 2. The waveform in panel a, obtained during interval 1, is non-sinusoidal with a characteristic frequency of ~45 -50 Hz and an amplitude of ~200 mV/m. Somewhat later, waveforms have, in addition, large amplitude variations near f_{cO}. Panel b(interval 2) shows another example of a non-sinusoidal waveform with a characteristic frequency near f_{cH} with a longer modulation near 10 Hz. Very nonlinear spikelets are often observed in similar upflowing electron regions [*Ergun et al.*, 1998]. The waveform during interval 3 (panel c) does not exhibit very clear frequency structure. The waveforms observed during interval 4 (panel d) are quite variable. At times, the waves are very coherent and sinusoidal; at other times, there are multiple frequencies and/or non-sinusoidal shapes.

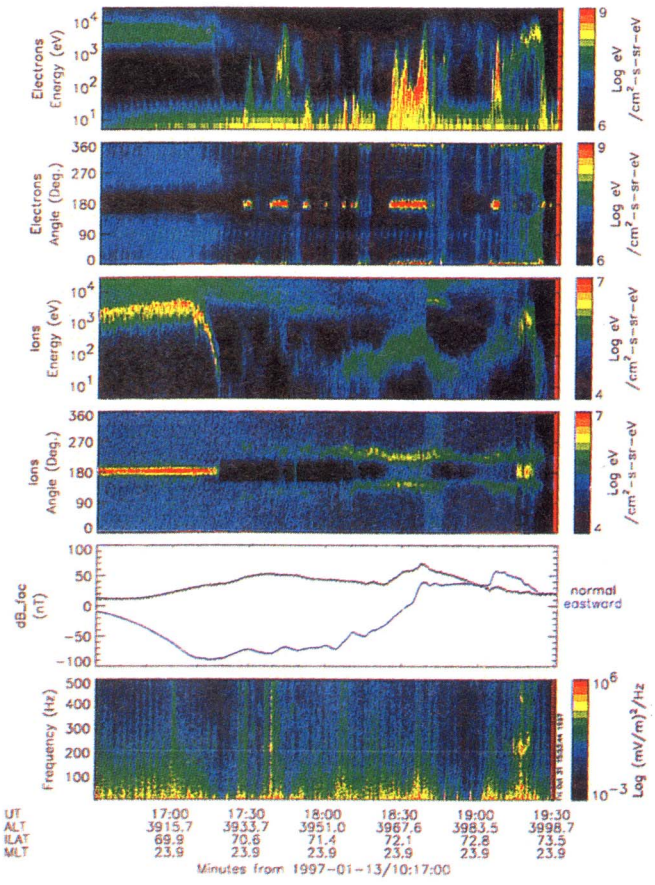

Figure 1. An overview of 3.5 minutes of data at 23.8 MLT in the auroral zone. (a) Electron energy spectrum; (b) Electron pitch angle spectrum; (c) Ion energy spectrum; (d) Ion pitch angle spectrum; (e) eastward and northward components of the magnetic field in field-aligned coordinates; and (f) Power spectrum of the electric field along the satellite velocity vector (~ perpendicular to the magnetic field). The hydrogen cyclotron frequency is the white line.

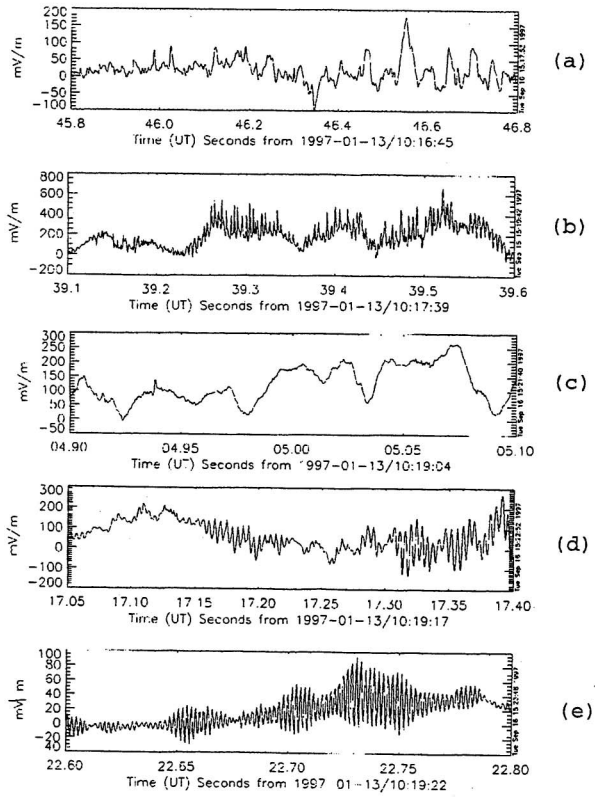

Figure 2. Sample electric field waveforms during the events of interest. Note sample durations differ.

3. Linear Dispersion Calculations

The linear stability of the plasma for the four events was examined by solving the electrostatic dispersion relation with particle distributions modeled as drifting bi-Maxwellians. The characteristics of the distribution functions for all species, during each of the four intervals, have been determined using several different methods. Plasma wave cutoffs provided checks on the total plasma density during some intervals. Parameters for the models which are most consistent with the particle and wave data are shown in Table 1. It should be noted that, while the ion beams are well-modeled by Maxwellians

Table 1. Parameters in Dispersion Calculation

	$n(cm^{-3})$		V_d(km/s)		$T_{\|}$(eV)		$T_{\perp}$(eV)	
Event #	1	2	1	2	1	2	1	2
Ion beams								
e-ps	0.4	0.8	0	0	3.4k	1.5k	3.4k	6.0k
e-beam	0.05	0.3	-9k	-8.9k	200	250	250	200
e-backgr.	0	0.1		0		20		20
H-ps	0.15	0.2	0	0	12k	4k	12k	16k
H-beam	0.15	0.5	644	617	100	400	270	400
O-beam	0.1	0.2	183	154	160	150	600	300
He-beam	0.05	0.3	302	308	214	200	275	200
UFEs								
e-beam	0.5	2	6.6k	5.9k	200	140	25	45
e-backgr.	0.1	0.5	0	0	10	20	10	20
H-ps	0.1	0.4	0	0	3.7k	5.0k	5.2k	5.0k
H-conic	0.27	0.41	0	0	80	400	380	400
O-conic	0.08	1.14	0	0	100	150	300	300
He-conic	0.15	0.55	0	0	100	200	200	200

and the moments for the beams and the inverted V electrons are well determined, the upflowing electrons are very non-Maxwellian and the moments are more uncertain. In addition, these parameters were not constant for the duration of any interval. Therefore, other model parameters, in addition to those in Table 1, were examined as discussed below.

Two sets of drifts were examined for each parameter set for the upward ion beams at 10:16:40 and 10:19:17. The first set was derived from the IESA energy spectrum of the total ion distribution function. It was assumed that the peak in the spectrum at zero pitch angle represents a common energy to which each ion component has been accelerated. The ratios of the ion beam drifts are equal to the square root of the mass ratio. The second set of drifts is the first velocity moment of each ion component from TEAMS data. These are not related by the square root of the mass ratio as discussed for a statistical data base by *Moebius et al.* [1998]. Each set of drifts was tested for stability since they represent the two extremes expected for the relative velocities of the various components. Several different sets of ion temperatures were also examined.

The primary differences between the observed parameters for the two ion beam events are that the plasma observations during the first event were consistent with the existence of no background electron population (see *Strangeway et al.*, 1998 for a discussion of regions with very low cold background density), a much lower total density, somewhat higher ion drifts, and lower current (corresponding to lower electron beam density). During the first ion beam event, the most intense waves were confined to low frequencies (<~50 Hz). Examination of the time series data provides evidence for waves with irregular waveforms with periodicities at <~15 and 45 Hz. Although the waves exhibited a broad spread in wavevector angles, they were primarily polarized perpendicular to the magnetic field. The observed waves were quite different during the second ion beam event when quasi-monochromatic waves near the helium and hydrogen cyclotron frequencies are both observed. Second harmonics of the hydrogen and helium cyclotron frequencies are also observed, as are modulations near the oxygen cyclotron frequency. There was a magnetic component (whose magnitude was very small (<0.5 nT) such that E/B>>c) during the most intense interval of waves near f_{cH}.

The results obtained from the dispersion relation calculation are consistent with the observations described above. In the first beam event (10:16:40), the electron drift excites electrostatic oxygen cyclotron waves nearly perpendicular to the magnetic field. The upward ion beams drive parallel propagating broadband waves, with the peak growth at ~45 Hz, through an ion-ion interaction excited by differential drift of the ion beams [*Bergmann et al.*, 1988]. Using the measured ion drifts reduces slightly the frequency at which the peak growth occurs, while increasing the ion beam temperature increases the damping of the ion-ion mode. For the case of the 10:19:17 event, the electron drift drives EHC waves with the peak growth at f= 1.02 f_{cH}. The most unstable wavelength is in good agreement with the wavelength obtained from an interferometric analysis. In addition, EOC and EHeC waves (at both the first and second harmonic) are unstable. The background electrons damp the ion-ion modes for this case. Because the determination of the density of background electrons is uncertain for this period, the dispersion relation was also examined assuming that there were no cold electrons. The main effects were to reduce the frequency of the most unstable electron drift driven EIC mode to 0.95 f_{cH} and to allow growth of parallel propagating ion-ion modes at <~20Hz. The observations are more consistent with the presence of some cold electrons. Although these numerical electrostatic results are consistent with the observed waves, there was a magnetic component during the most intense EHC wave observed. The electromagnetic dispersion relation for these parameters will be discussed in a future publication.

We looked for conditions under which EIC waves might be driven by the ion beams at 10:19:17. However, the only unstable beam-driven waves were parallel propagating. These results show that the observations are inconsistent with a beam-driven mechanism for the waves near the cyclotron frequency, and are consistent with current-driven waves.

Both upflowing electron events were associated with intense downward currents, and had very similar temperatures and drifts for both the electrons and the ions. The second event, at 10:19:05, had a much higher total density and higher oxygen percentage. In addition, there were countersteaming electrons. The upflowing electrons during the first event, at 10:17:40, had a higher drift speed and, in addition, a clear beam structure in the distribution function with fewer electrons below the peak in comparison to 10:19:05. For both events, the drift shown in Table 1 and used in the dispersion relation is less than the first moment of the electron distribution. The lower value is used because the observed distributions have a long high velocity tail and because, for the 10:17:40 case, the peak is at a lower velocity. The cold background density is not well determined for these events.

The waves during the first upflowing electron beam event were extremely intense with broadband power up to ~1 kHz. In addition, there was a strong peak near f_{cH} and a weak one near f_{cHe}. Examination of the waveforms (Fig. 2b) indicates that some of the broadband power is due to the non-sinusoidal shape of the EHC waves. There are simultaneous solitary waves in the parallel direction as described, for other upflowing electron events, by *Ergun et al.* [1998]. In contrast, during the second upflowing electron event, intense waves were limited to frequencies <100 Hz, with weak power just above f_{cH} appearing very briefly (< few tenths of a second).

For the Table 1 parameters for the 10:17:40 event, the calculation indicates that both EHC and EHeC waves are destabilized near 90 degrees by the electron drift. The linear growth rates for this oblique electron-ion mode, however, are much less than the broadband parallel electron-acoustic instability which extends from a few Hz through ~1500 kHz. It is possible that it is the electron acoustic mode that grows nonlinearly to produce the solitary waves observed in this region. The mode is dependent on both the drift and the existence of the cold population. Reducing the drift reduces the maximum unstable frequency. If the cold electron background is removed, the electron acoustic waves are not present, the EHeC waves have the largest growth rate, there are no EHC waves, and there is a low frequency (<16 Hz) parallel instability. This is inconsistent with the observed waves, which favors the existence of a cold background population in this event, although it is possible that using model distributions closer to the actual ones would modify this conclusion. The effects of the temperatures and temperature anisotropy of the upflowing beam have also been examined. For a reasonable range of these parameters, the instability is not affected. Even increasing the anisotropy to $T_{\perp}/T_{\parallel}=1/25$ has

no effect on the electron drift-driven waves, and, in the absence of a drift, does not destabilize waves.

Unlike the 10:17:40 event, there is no 'gap' visible in the energy spectrum between the upflowing electrons and background electrons in the 10:19:05 event. Further, there is a counterstreaming component which is also not present in the 10:17:40 case. Both features decrease the positive slope on the beam available to drive waves. They are modeled by using a larger background electron temperature and a lower drift velocity for the electron beam for 10:19:05 compared with 10:17:40. The higher temperature of the cold background electrons in the 10:19:05 event increases the damping of the electron acoustic and the ion cyclotron modes. The unstable modes depend on the drift velocity. Taking the electron beam speed to be 7000 km/s as indicated by the first moment of the upgoing distribution, EHC, EOC and EHeC waves are destabilized with low growth rates. However, there was no peak in the observed distribution at that velocity. Lowering the drift to 5900 km/s results in a region of instability from ~26 Hz to ~160 Hz with the maximum growth rate at a frequency of 56 Hz near 90 degrees. The growth rates are about 1/100 the growth rates found for the parameters in the 10:17:40 event.

There is reasonable agreement between the linear dispersion relation results for the two upflowing electron beam events and the observations, especially given the limitations of the model distributions and the fact that the waveforms are very nonlinear. The numerical results show large growth rates for EIC waves and broadband electron acoustic waves in the first event, but only small growth rates over a much more limited frequency band in the second event.

4. Discussion and Conclusions

The high resolution data from FAST have, for the first time, clearly identified the electron drift (i.e. field-aligned current) as the source of free energy to drive electrostatic ion cyclotron waves in regions containing both ion beams and field-aligned currents in the specific auroral zone crossing examined. This is consistent with the conclusions of *Cattell et al.* [1991]. The ion beams can drive lower frequency ion-ion instasbilities in the case where there are no background electrons to damp the waves, as was observed in the ion beam event at 10:16:40. Although these waves sometimes can have peak growths near the cyclotron frequency of the various ion species, they are parallel propagating in contrast to the oblique EIC waves. In the upward electron region, the results are also consistent with the electron drift being the free energy source for EIC modes, although, in this region, both the moments calculations and the distribution function model are less accurate than in the ion beam regions. The upflowing electron drift also destabilizes broadband parallel electron acoustic waves via an electron-electron interactions when a cold background electron population is present. If the relative drift is too small, then the unstable modes are oblique lower frequency ion acoustic modes. The observed waves in both the ion and electron beam regions are consistent with the linear dispersion calculations. It must be noted, however, that the observed waveforms are often highly non-sinusoidal indicating the desirability of simulations to examine the evolution of the waves and plasma. In addition, there were weak magnetic components associated with some of the waves which can not be modeled by the electrostatic code. Studies of other auroral zone crossings [*Chaston et al.*, 1998; *McFadden et al.*, 1998] have shown the occurrence of spectral features in the waves in both the uflowing electron regions and the ion beam regions which are different from those described herein. Therefore, future work will include a statistical study of the waves and particles to determine for what range of plasma parameters the results obtained in this specific event are more generally applicable, as well as improved distribution models.

ACKNOWLEDGMENTS. The authors thank the NASA FAST spacecraft and operations teams, the instrument engineering and software teams at UCB, LMRL, UNH and UCLA, and the SOC team at UCB. This work was supported by NASA Grant NAG5-3596 and by the Minnesota Supercomputer Institute.

References

Andre, M et al., Ion waves and upgoing ion beams observed by Viking, *Geophys. Res. Lett., 14*, 463, 1987.

Bergmann, R., Electrostatic ion (hydrogen) cyclotron and ion acoustic wave instabilities in regions of upward field-aligned current and upward ion beams, *J. Geophys. Res., 89*, 953, 1984.

Bergmann, R., I. Roth, and M. K. Hudson, Linear stability of the H+-O+two-stream interaction in a magnetized plasma, *J. Geophys. Res., 93*, 4005, 1988.

Boehmer, H., et al., Ion-beam excitation of electrostatic ion-cyclotron waves, *Phys. Fluids, 19*, 340, 1976.

Carlson, C. et al., The FAST Auroral Snapshot mission, this issue, 1998a.

Carlson, C. et al., FAST observations in the downward auroral current region: Energetic up-going electron beams, parallel electric fields, and ion heating, this issue, 1998b.

Cattell, C. A. , The relationship of field-aligned currents to electrostatic ion cyclotron waves, *J. Geophys. Res., 86*, 3641, 1981.

Cattell, C.A et al., ISEE 1 Observations of EIC Waves in Association with Ion Beams on Auroral Field Lines From ~2.5 to 4.5Re, *J. Geophys. Res., 96*, 11421, 1991.

Chaston, C. et al., Characterstics of electromagnetic proton cyclotron waves along auroral field lines observed by FAST in regions of upward current, this issue, 1998.

Dusenbery, P. et al., Ion-ion waves in the auroral region: Wave excitation and ion heating, *J. Geophys. Res., 93*, 5655, 1988.

Ergun, R. et al., FAST satellite observations of large amplitude solitary waves, this issue, 1998.

Ganguli, G. et al., *Phys. Fluids, 31*, 823, 1988.

Kaufmann, R. L. et al., Interaction of auroral H+ and O+ beams, *J. Geophys. Res., 91*, 10,080, 1986.

Kindel, J. M., and C. F. Kennel, Topside current instabilities, *J. Geophys. Res., 76*, 3055, 1971.

Kintner, P. M., On the distinction between EIC waves and ion cyclotron harmonic waves, *Geophys. Res. Lett., 7*, 585, 1980.

Kintner, P., M.Kelley, and F. Mozer, Electrostatic hydrogen cyclotron waves near one earth radius altitude in the polar magnetosphere, *Geophys. Res. Lett., 5*, 139, 1978.

Kintner, P. M. et al., Simultaneous observations of energetic (keV) upstreaming ions and EHC waves, J. Geophys. Res., 84, 7201, 1979.

Lysak, R. L., and M. A. Temerin, Generation of Alfven-ion cyclotron waves on auroral field lines in the presence of heavy ions, *Geophys. Res. Lett., 10*, 643, 1983.

Lysak, R. et al., Ion heating by strong electrostatic ion cyclotron turbulence, *J. Geophys. Res., 85*, 678, 1980.

McFadden, J. et al., Electron modulation and ion cyclotron waves observed by FAST, this issue, 1998.

Moebius, E. et al., Species Dependent Energies in Upward Directed Ion Beams Over Auroral Arcs as Observed with FAST TEAMS, this issue, 1998.

Temerin, M. A., and R. L. Lysak, Electromagnetic ion cyclotron mode (ELF) waves generated by auroral electron precipitation, *J. Geophys. Res., 89*, 2849, 1984.

Temerin, M. et al., Nonlinear steepening of the electrostatic ion cyclotron wave, *Phys. Rev. Lett., 43*, 1941, 1979.

C. Cattell and K. Sigsbee, School of Physics, 116 Church St. SE, University of Minnesota, Minneapolis, MN 55455 (e-mail: cattell@belka.space.umn.edu)

(Received November 18, 1997; accepted January 13, 1998.)